In-orbit characterization of radio-frequency ion micropropulsion in Taiji-1

Longfei Ma,[1,*] Jianwu He,[1,2,*] Chao Yang,[1] Chu Zhang,[1] Li Duan,[1,2] Qi Kang,[1,2] Peng Liu,[3] Yongli Yin,[4] Xuequan Zhang,[5] Shuang Yang,[5] Aibing Zhang,[5] Yifang Xie,[5] Changbin Xue,[5] and Zhi Wang[6]

[1]*Micro Gravity Key Laboratory, Institute of Mechanics, Chinese Academy of Sciences, Beijing, China*
[2]*School of Engineering Sciences, University of Chinese Academy of Sciences, Beijing, China*
[3]*Department of Physics and Tsinghua-Foxconn Nanotechnology Research Center, Tsinghua University, Beijing, China*
[4]*China Astronaut Research and Training Center, Beijing, China*
[5]*National Space Science Center, Chinese Academy of Sciences, Beijing, China*
[6]*Fine Mechanics and Physics, Changchun Institute of Optics, Chinese Academy of Sciences, Changchun, China*

(Received 14 June 2024; revised 18 February 2025; accepted 13 April 2025; published 12 May 2025)

The "Taiji program in space" for space-based gravitational wave detection will open a window for observing gravitational waves in the mid-to-low-frequency range (0.1 mHz to 1 Hz). Taiji-1 satellite as the inaugural satellite, was launched on 31 August 2019, to validate several critical technologies. The radio-frequency ion micro-propulsion (RMP) as a primary propulsion system underwent in-orbit flight validation. All four thrusters successfully completed crucial performance tests. This paper will present the primary in-orbit test results. It is found that the thrust range of the RMP is 5 μN to 52 μN. When a thrust of 50 μN, the thrust noise is approximately 0.4 $\mu N/\sqrt{Hz}$ (10 mHz–1 Hz), which is 2 to 4 times that of low-thrust (5 μN). The thrust response time is about 20 ms. The characterization of RMP in orbit has reached the expectations of Taiji-1 satellite mission. The current in-orbit performance (thrust resolution, thrust noise and lifetime) of the RMP falls short of the goals set by the "Taiji program in space" and requires further enhancement.

DOI: 10.1103/PhysRevD.111.103023

I. INTRODUCTION

The "Taiji program in space" is a space science mission proposed by the Chinese Academy of Sciences to detect space gravitational waves and unveil the nature of gravity [1]. According to the detection principle, this program involves several key technologies, including intersatellite laser interferometry system, drag-free control system, ultrastability satellite system, etc. [2]. There will be three steps to realize the gravitational waves in space, and Taiji-1 satellite as the key technology verification satellite for the first run of the "Taiji program in space" has realized the in-orbit verification of multiple key technologies for future space gravitational wave detection, among which the radio-frequency ion micropropulsion (RMP) is one of them [3].

Space gravitational wave detection is based on the Michelson interferometer measurement principle, which utilizes laser interferometry to precisely measure the changes in optical path caused by gravitational waves. There will be three satellites flying in a triangular formation for gravitational waves detection, and each satellite will take two test masses. The laser propagates between the test masses and establishes the laser interference link between the two satellites. When the gravitational wave passes by, the optical path between the pairwise test masses changes and is read out by the laser interference signal. During the formation flight in space, the satellites are subject to nonconservative forces such as solar radiation pressure, solar wind or other cosmic rays. The utilization of drag-free control technology can ensure that the distance between the test masses and the satellite remain in equilibrium and maintain the inertial motion of the test masses, with the satellite micropropulsion system serving as the actuator [2]. There are many micropropulsion technologies that can be applied to space gravitational waves detection, but each has advantages and disadvantages [4]. ESA's LISA Pathfinder was launched in December 2015, which carried 12 cold-gas thrusters developed by ESA and 8 colloid thrusters developed jointly by NASA and the Busek Corporation. The cold-gas thrusters are distributed on three external panels of the satellite, with four thrusters installed on each panel, two of which serve as primary thrusters while the others as redundant backup thrusters. They are controlled using piezoelectric actuators to regulate mass flow rate and thrust, with each thruster capable of providing thrust ranging from 0 to 500 μN. The thrust resolution is 0.08 μN, and the thrust noise level is 0.17 $\mu N/\sqrt{Hz}$ (0.3 mHz–10 mHz), with a specific impulse of approximately 70 s [5]. However, the low specific impulse is the primary drawback of cold-gas thrusters. The eight colloid

[*]These authors contributed to the work equally and should be regarded as co-first authors.

thrusters as two assemblies are arranged symmetrically on the top and bottom panels of the satellite; with each thruster having a thrust range of 5 μN to 30 μN and a thrust resolution better than 0.1 μN, the thrust noise reaches 0.1 μN/$\sqrt{\text{Hz}}$ (0.1 mHz–0.1 Hz). Each cluster has a power of approximately 17 W and a weight of 14.8 kg [6,7]. In the "Taiji-1" satellite, there are four Hall Micro thrusters (HMTs), and each thruster has two working modes (cold-gas mode and accelerated plasma mode) [8]. The cold-gas mode was just aimed to expand the range of thrust, but the specific impulse was low. In cold-gas mode, the thrust range is from 0.1 μN to 150 μN, while in accelerated plasma mode, it ranges from 5 μN to 100 μN. The thrust resolution is 0.7 μN, and the thrust noise is better than 0.6 μN/$\sqrt{\text{Hz}}$ (0.01 Hz–1 Hz), with a power of approximately 5 W. To meet the requirements of space gravitational wave detection, further improvement is needed in thrust resolution and thrust noise. TianQin project was initiated in 2014 by Luo for gravitational waves detection in space [9]. The "TianQin-1" satellite, launched on 20 December 2019, verified the in-orbit performance of cold-gas microthrusters. The thrust range is from 1 μN to 60 μN, with a thrust resolution of 0.1 μN. At a frequency of 0.1 Hz, the thrust noise is 0.3 μN/$\sqrt{\text{Hz}}$, with a specific impulse of approximately 60 s, slightly inferior to that of LISA Pathfinder cold-gas thrusters [4].

In the "Taiji-1" satellite, four radio-frequency ion microthrusters (μRIT) of the RMP combines inductive-coupled plasma discharge and ion extraction focusing, offering advantages such as high specific impulse, long life, and rapid thrust response compared to cold-gas and Hall-effect microthrusters. Research on an radio-frequency ion thruster was initiated at Giessen University in 1960. After more than half a century of development, this technology has undergone space flight verification and in-orbit application [10–12]. Targeting space gravitational wave detection missions, the RIT-μX developed by Giessen University has a thrust range of 10 μN to 120 μN, a thrust resolution of 0.1 μN, and a thrust noise of 0.1 μN/$\sqrt{\text{Hz}}$, meeting all requirements except for the lower limit of thrust [13]. Busek Corporation, under NASA sponsorship, developed the BIT-1 engineering prototype, capable of thrust up to 180 μN, with a thrust resolution of 0.1 μN and an optimal specific impulse of 2150s, with power consumption of about 10W. However, the key performance of thrust noise has not been disclosed [14].

TABLE I. The requirement of Taiji program.

	Taiji [5]	Taiji-1
Thrust range (μN)	5–50	5–50
Thrust noise (μN/$\sqrt{\text{Hz}}$)	0.1 (0.1 mHz–1 Hz)	1.5 (10 mHz–1 Hz)
Thrust resolution (μN)	0.1	1.5
Thrust response time (ms)	50 (50 μN)	50 (25 μN)
Lifetime (h)	10000	···

The "Taiji-1" satellite was launched on August 31, 2019 [3]. The RMP as the first batch of in-orbit test payloads, completed a thrust test, thrust range test, and thrust response time test from September 2019 to March 2020. This paper will provide detailed results of the in-orbit performance testing of RMP, indicating the optimization direction for propulsion to meet the requirements of space gravitational wave detection in Table I.

II. RMP HARDWARE

The RMP consists of four radio-frequency ion thrusters (μRIT-1) with a discharge chamber inner diameter of 1 cm, a power processing unit (PPU), a high-precision micro-mass-flow control unit (μMFC), and two clusters of carbon nanotube neutralizers (CNTN), as showed in Fig. 1. Each

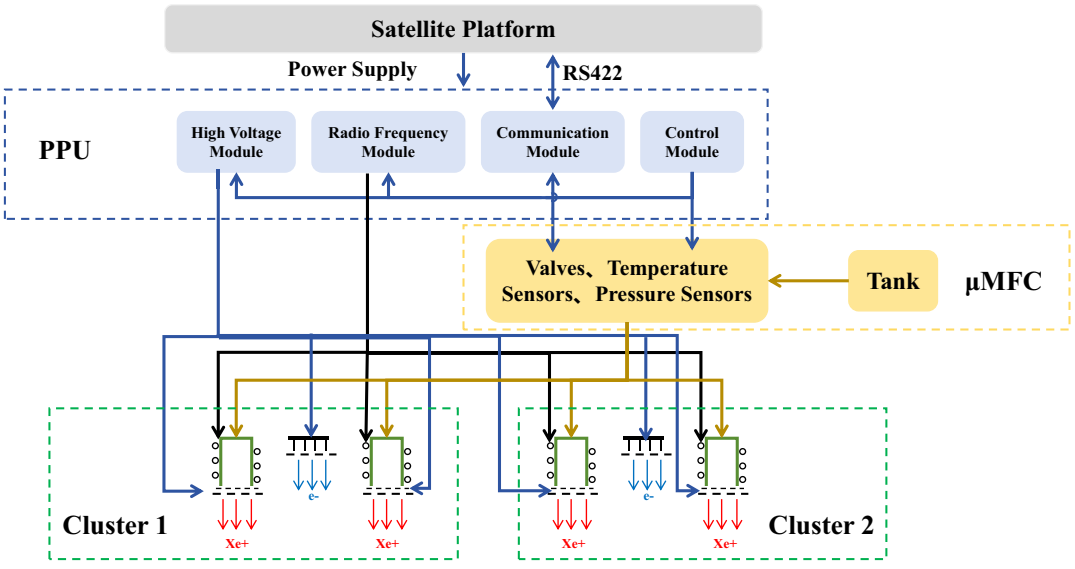

FIG. 1. The component of RMP, consisting of 2clusters of μRIT-1, a PPU, and a μMFC.

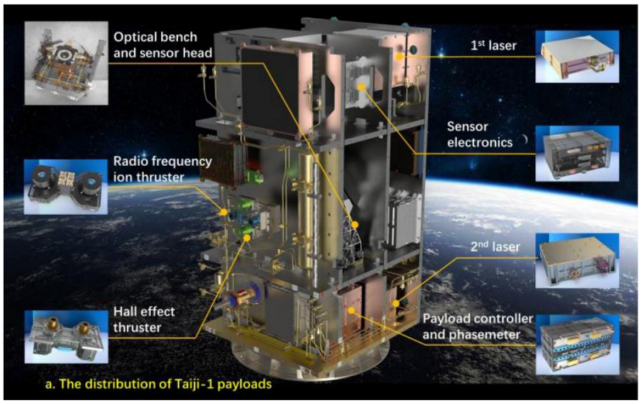

FIG. 2. The distribution of Taiji-1 satellite payloads [15]. The two μRIT-1 are shown with two Hall effect micro-thrusters.

cluster comprises two μRIT-1 and one CNTN, and two clusters were installed on opposite side, as showed in Fig. 2 [14].

The μRIT-1 comprises a discharge chamber, a radio-frequency antenna, an ion optical system, a gas inlet, a shielding enclosure, and a mounting substrate. The radio-frequency network matching is embedded inside the mounting substrate to reduce power loss, as showed in Fig. 3(a).

The CNTN operates based on the field emission principle, where a strong electric field between the grid and emitter extracts electrons. A cluster CNTN consists of four modules, each comprising an emitter, a grid, a mounting base, and an insulating layer. The ultra-aligned carbon nanotubes thick film undergoes high-temperature and

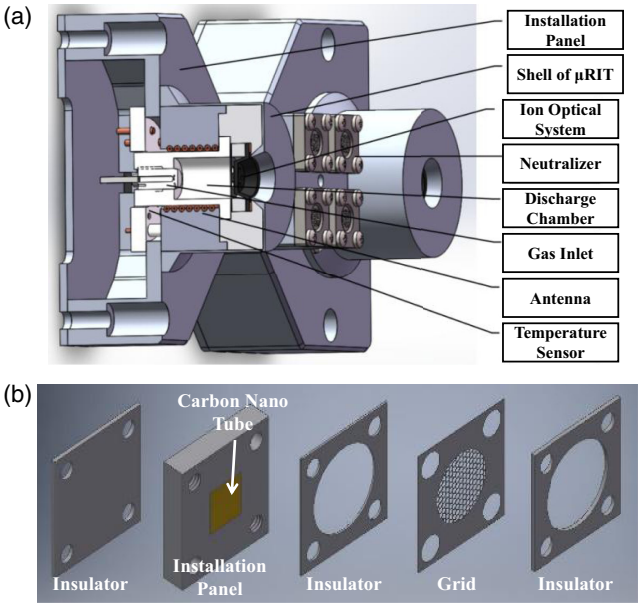

FIG. 3. Structure of μRIT-1 and CNTN, the μRIT-1 includes installation panel, shell of μRIT, ion optical system, neutralizer, discharge chamber, gas inlet, antenna, and temperature sensor, the CNTN includes insulators, installation panel, carbon nano tube, insulator, and grid.

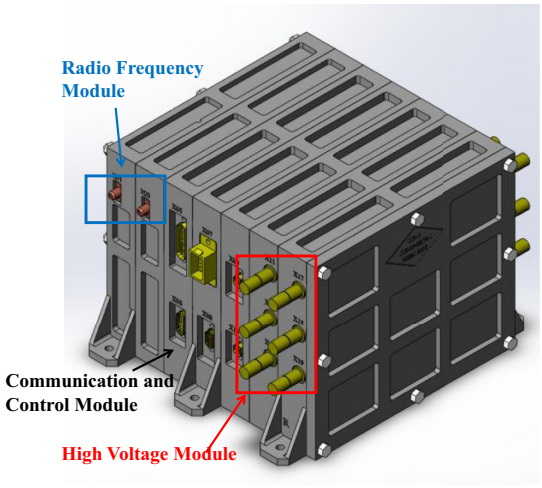

FIG. 4. The PPU of RMP. In order to avoid electromagnetic interference of radio frequency source, the high-voltage circuit boards and radio-frequency circuit boards are designed on both sides of the PPU.

high-pressure densification treatment and surface processing to the same size. The four modules are controlled by one high-voltage source and installed between two μRIT-1 to achieve electrical neutrality, as showed in Fig. 3(b) [16].

The PPU integrates a control module, a communication module, a high-voltage module, and a radio-frequency circuit module, consisting of seven circuit boards, as showed in Fig. 4. The radio-frequency circuit module provides four-channel output with an adjustable frequency range of 9 MHz to 9.5 MHz. The power output is approximately 38 dBm, with power fluctuation less than 0.2 dB. The high-voltage module comprises six outputs, independently controllable, with each channel capable of outputting from 300 V to 2000 V, meeting real-time adjustability requirements in-orbit. The PPU installs on the position close to the +Z side, in proximity to one cluster of thrusters. Communication is conducted using RS422.

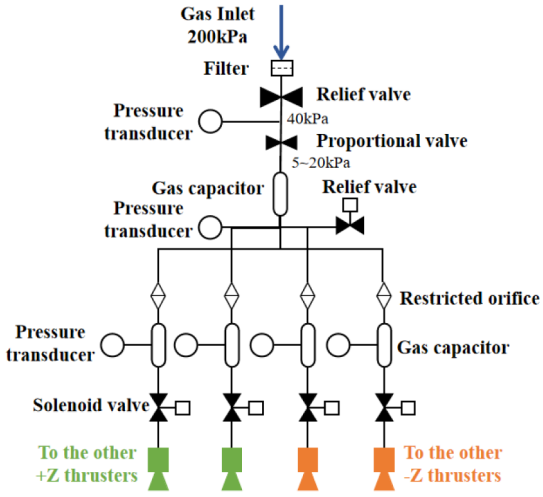

FIG. 5. Schematic of μMFC.

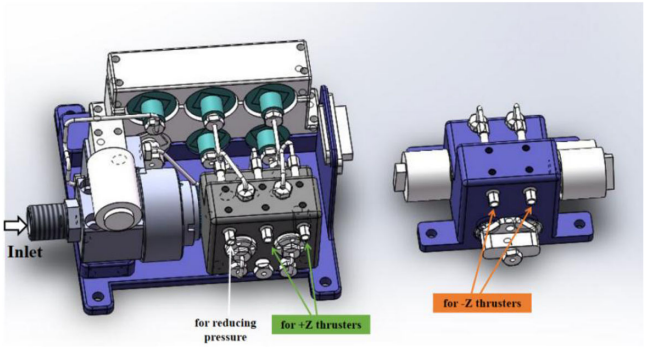

FIG. 6. Structure of μMFC.

The μRIT-1 requires the μMFC to provide approximately 10 μg/s of propellant flow, with an adjustment accuracy of 1 μg/s. One high precision μMFC simultaneously supplies propellant flow to four μRIT-1, structurally comprising a pressure regulation module, a gas supply module, and a measurement module. It employs 20 μm restricted orifices to achieve micro-mass-flow control by adjusting the pressure difference before and after the restricted orifice. The μRIT-1 utilizes pulse gas pressure discharge to ignite, and a 1 mL gas capacitor is designed before the solenoid valve, as showed in Fig. 5. To accommodate the installation of thrusters, two propellant supply lines are integrated with the pressure regulation module, while the other two propellant supply lines are independently installed near the thrusters, as shown in Fig. 6.

III. PROPULSION CHARACTERIZATION

The "Taiji-1" satellite serves as a verification platform for key technologies in space gravitational wave detection. The RMP conducted a total of 69 operating conditions with 128 tests. This paper primarily analyzes the test results of ignition, thrust test, thrust noise, and thrust response time.

A. Thruster ignition

The RMP adopts a pulse propellant discharge to ignite. After setting the radio-frequency power, the grid voltage, and the propellant pressure in the gas path, opening the solenoid valve at the front of the thruster will generate a pulse propellant flow into the discharge chamber and the ion optical system. According to Paschen's law [17], the discharge between the grids is related to factors such as the grid voltage V, material, gas type, gas pressure p, and grid electrode spacing d. The discharge threshold voltage is given by

$$V_{bd} = \frac{B \cdot pd}{\ln \frac{A \cdot pd}{\ln(1+1/\gamma)}}, \tag{1}$$

where γ is Townsend's second ionization coefficient; it is about 8.766 with RMP parameters, and A and B are the constants related to the gas species, 3.58 $\mathrm{cm}^{-1}\,\mathrm{Torr}^{-1}$ and $-351.7\ \mathrm{V}\cdot\mathrm{cm}^{-1}\,\mathrm{Torr}^{-1}$ with Xe.

The screen grid voltage and the gas capacitor pressure serve as critical parameters for in-orbit ignition test of the RMP. The ignition status of the thruster was verified under conditions of screen grid voltage ranging from 1200 V to 1700 V, acceleration grid voltage connecting 0 V, and gas capacitor pressures ranging from 9 kPa to 11.2 kPa, as showed in Fig. 7.

Before the ignition test, a preignition was conducted based on the RMP ignition conditions to confirm the propulsion status and ensure the smooth progress of the test. During the test, the screen grid ignition voltage value and the gas capacitor pressure was preset. When the pulse propellant passed through the strong electric field between the grids, an electron avalanche and Townsend discharge occurred. A large number of electrons entered the discharge chamber under the influence of the electric field and ionized propellant atoms, thereby igniting the thruster.

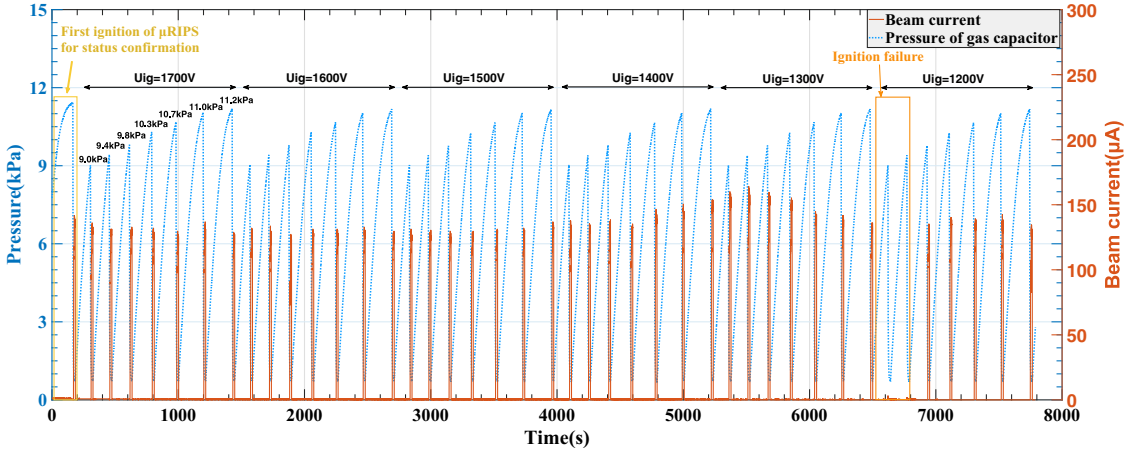

FIG. 7. Ignition test of RMP in-orbit. The red lines indicate the beam current of propulsion system after igniting. The blue lines indicate the pressure variation of gas capacitor when igniting.

To avoid any adverse effects on the satellite during the test, the screen grid voltage was controlled to 300 V after thruster ignition, then the thruster was shut down, entering the next operational condition test.

The test results indicate that when the gas capacitor pressure is set to 9.8 kPa or above and the screen grid voltage reaches 1200 V to meet the discharge threshold voltage, the RMP can achieve in-orbit ignition with a success rate of 100%. When the screen grid voltage is below the discharge threshold voltage, the thruster does not operate normally, and there is no ion beam. This ignition method enables the propulsion to be ignited within 250 ms, facilitating the rapid execution of space gravitational wave detection tasks. Traditional ignition by positive voltage of ion optical system attracting electrons from neutralizer, the PPU need an additional positive voltage circuit for acceleration grid. Although the ignition method in this paper can simplify the PPU, it may cause surface damage to the grid material, affecting the stability and life of the thruster, as discussed in Ref. [18]. Therefore, this ignition method is suitable for short-term or single-time ignition for long-term space missions, effectively reducing the complexity of the propulsion.

B. Thrust test

In ground-based experiments, the RMP completed thrust calibration using a micro-Newton thrust measurement system [3], which corrected the coefficient η in Eq. (2). During in-orbit thrust test, the acceleration of the satellite was measured by a gravity reference sensor (GRS) to measure the actual thrust of the RMP in conjunction with the satellite mass (183 kg), rather than operating in the inertial sensing mode. The GRS measures the displacement and acceleration of test mass in real time in line with the basic principle of capacitance displacement sensing [19]. In this test, GRS measurement results is the mean of three group data. The four thrusters are individually controlled by PPU and μMFC. While each thruster can be independently controlled, thrust adjustment is achieved by controlling the screen grid voltage, while maintaining constant propellant flow and radio-frequency power values, as detailed in Table II. Considering the mutual interference between the four-channel radio-frequency power output, the four thrusters were divided into three modes for thrust test. In this test, the actual thrust of a single thruster, two thrusters on the same side, and four thrusters operating simultaneously were tested and compared with the calculated thrust values. This test will adopt an open-loop control mode (the screen grid voltage was not adjusted according to the beam current for the command thrust),

$$F = \eta \times I \times \sqrt{\frac{2 \times V_b \times M}{q}} \tag{2}$$

$$\eta = \cos\frac{\pi V_b}{24000}, \tag{3}$$

where η is thrust calculation coefficient and depend on the V_b, I is ion beam current, V_b is ion optical system voltage, M is mass of propellant particle, and q is charge of each ion.

In the thrust tests, the thrust commands were sent by the satellite to the control module of the PPU. According to the Eq. (2), the thrust is used to determine the corresponding V_b and I. We assume that the xenon flow rate and RF power of each thruster remain consistent with the ground thrust calibration process, meaning that I remains unchanged and only V_b needs to be determined. Therefore, upon receiving the thrust commands, the four thrusters adjust V_b to achieve the desired thrust variation. However, the operating conditions of the PPU and μMFC in orbit differed slightly from those on the ground, such as variations in RF power output and xenon flow rate, which cannot be identified with high precision from the data. As a result, there were deviations in I for each thruster, leading to discrepancies between the calculated thrust and the thrust command.

1. Single thruster

Based on the results measured by the GRS, the thrust generated by the μRIT-1 B1 and B2 is positive, while that generated by A1 and A2 is negative, as illustrated in Figs. 8–10. In the single thruster test, each of the four thrusters was individually ignited, with thrust commands (red line) ranging from 0 μN to 50 μN, and steps of 0.5 μN, 1 μN, 1.5 μN, and 2 μN were applied at both ends to test the thrust resolution capability, as shown in Table III. But the GRS is subject to thrust measurement drift due to environmental influences on the satellite. As in Fig. 8(a), the measured thrust (green line) at 52 μN was not stable and slightly descended, and the measured thrust amplitude was up to 2 μN. Therefore, the thrust test is designed with a thrust increase steps and a thrust decrease steps to zero to eliminate GRS measurement errors. In addition, The GRS measurement results cannot clearly identify the

TABLE II. Parameters of RMP.

Parameters	B1	B2	A1	A2
V_b (V)		300–2000		
Frequency (MHz)	9.285	9.28	9.3	9.285
Propellant flow (sccm)		~0.08		
Radio-frequency power (W)	5	5	5.02	5.02

TABLE III. Thrust commands of single thrusters.

Thrust command (μN)	0	5	5.5	6.5	8	10	20	30	40	42	43.5	44.5	45	50
	50	45	44.5	43.5	42	40	30	20	10	8	6.5	5.5	5	0

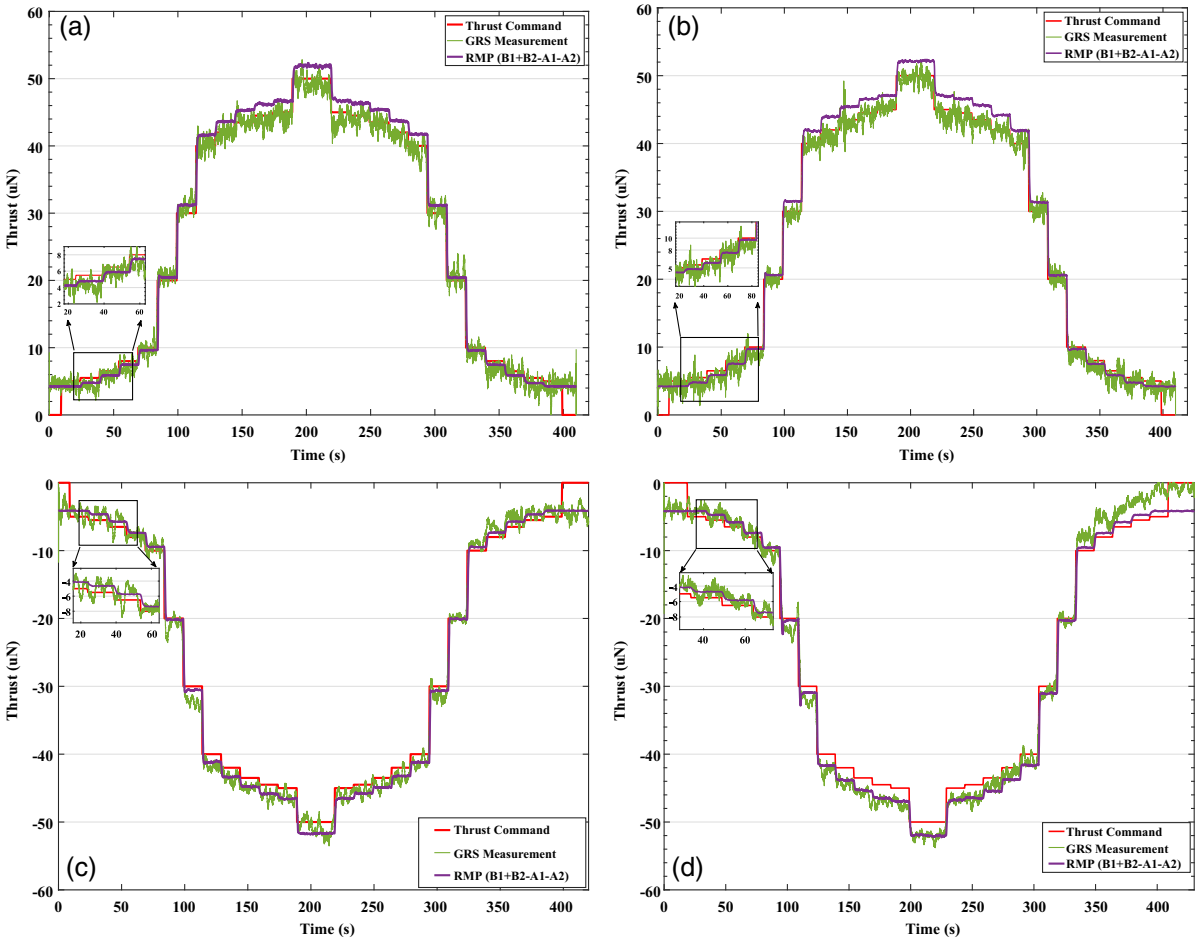

FIG. 8. RMP calculated thrust and GRS measurement thrust of single thruster operating. (a) thruster B1 measurement, (b) thruster B2 measurement, (c) thruster A1 measurement, and (d) thruster A2 measurement.

corresponding thrust steps, especially in the case of low thrust. Moreover, the measured thrust fluctuates significantly within each thrust step.

From the calculated thrust results (purple line), four μRIT-1 can achieve a resolution of 0.5 μN, and they satisfy both low and high thrust values. The GRS can identify thrust resolutions of 1 μN within the thrust range, but it cannot measure thrust at 0.5 μN, as shown in Figs. 8(a) to 8(c). This inability may be due to measurement drift obscuring small changes in thrust values. Additionally, both calculated thrust values and GRS measurement thrust values indicate that four μRIT-1 can achieve variable thrust ranging from 5 μN to 52 μN. In comparison with ground-based measurements, the thrusts of the four thrusters in-orbit are consistently lower, exhibiting deviations ranging from 1 μN to 2 μN. During ground-based experiments, factors such as vacuum scale limitations, temperature drift, and cable perturbations contribute to error in the obtained results, but the results are more reliable due to the measurement method and the calibration of torsional pendulum [4].

Furthermore, in Fig. 8, it can be observed that the fluctuation amplitude of the calculated thrust relative to the GRS measured thrust is smaller. This indicates that the voltage applied to the screen grid and the ion beam value are relatively stable. Conversely, external disturbances affecting the satellite platform result in the GRS measurement results containing much additional information, leading to larger fluctuations in the thrust measurement results.

2. Double thrusters

Figure 9 presents the results of simultaneous thrust test of two thrusters. Similar to the single thruster test, both cluster of thrusters (B1 and B2, and A1 and A2) incrementally increase thrust from 5 μN to 52 μN in a stepwise manner and simultaneously output the same thrust in Table IV. Since the GRS measures the total thrust of a cluster of thrusters on the same side, the calculated thrust

TABLE IV. Thrust commands of double thrusters.

Thrust commands (μN)	0	12	16	20	24	28	32	36	40	50	60	70	80	90	100	110
	110	100	90	80	70	60	50	40	36	32	28	24	20	16	12	0

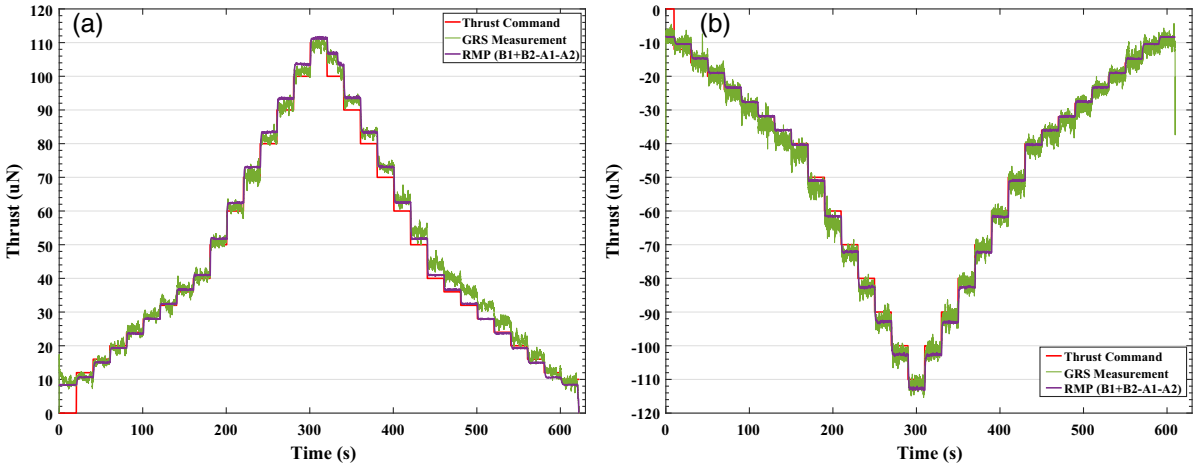

FIG. 9. Calculated thrust and GRS measurement thrust of double thrusters operating. (a) thrusters B1 and B2 measurement and (b) thrusters A1 and A2 measurement.

(purple line) also compares with the measured results (green line).

From the Fig. 9, it is observed that there is a high consistency between the calculated thrust and the measured thrust values. Even with individual thrusters generating thrust changes as small as 0.5 μN, they meet the GRS measurement threshold of 1 μN thrust change. Compared to the results of single thruster test, the total thrust of two thrusters simultaneously is slightly higher than the sum of the thrust of individual thrusters, ranging from approximately 2 μN to 10 μN. In the thrust test of B1 and B2, the thrust increase is attributed to the increase in screen grid voltage and ion beam of thruster B2, leading to an increase in the total thrust. Similarly, in the thrust test of A1 and A2, the increase in screen grid voltage for both A1 and A2 leads to an increase in the total thrust. The reason of thrust difference between double thrusters mode and single thruster mode is the simultaneous operation of two thrusters causes mutual interference in the internal high-voltage modules of the PPU. Since this test was conducted in open-loop control mode, the beam current cannot be fed back to the PPU to adjust the output of the screen grid voltage, resulting in the output voltage higher than the voltage required for command thrust.

3. Full thrusters

Figure 10 shows the result of simultaneous thrust test of four thrusters, using the same stepwise thrust increments where each thruster gradually increases thrust from 5 μN to 50 μN and outputs the same thrust. However, in this test, the GRS is unable to measure the actual thrust of each thruster or the total thrust of thrusters on the same side. Therefore, only the calculated thrust values for each thruster are analyzed.

Each thruster can achieve thrust ranging from 5 μN to 50 μN. Below 25 μN, the thrusts of the four thrusters are essentially consistent. However, as thrust increases, the thrusts of A2 and B2 are slightly higher than that of A1 and B1. At maximum thrust, the thrust difference reaches 3 μN. The main reason for this difference is the variation in the radio-frequency power, resulting in a difference of

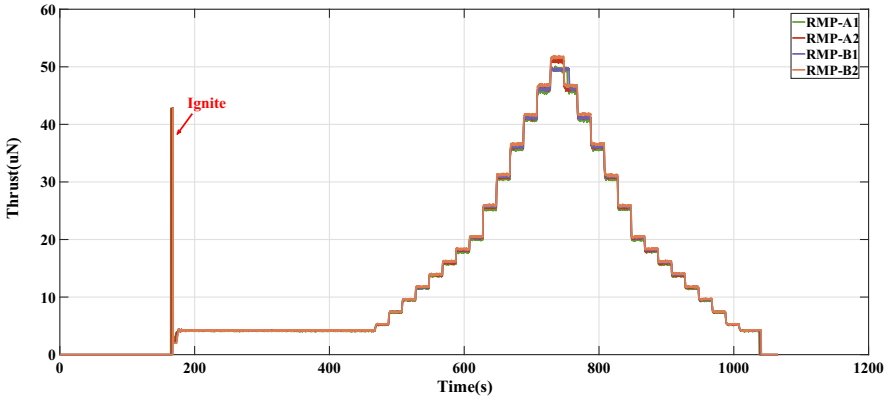

FIG. 10. Calculated thrust and GRS measurement thrust of full thrusters operating.

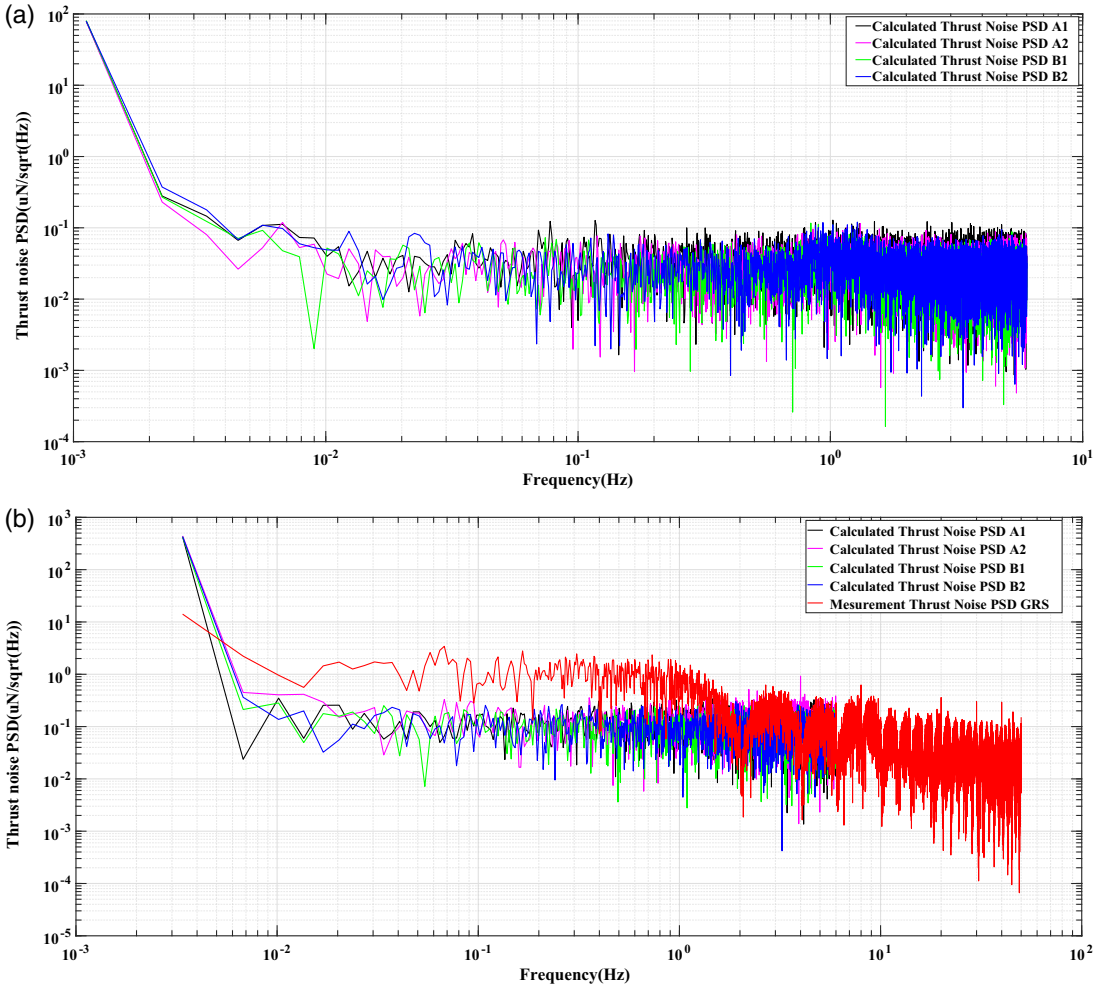

FIG. 11. Thrust noise power spectral density when full thrusters operating synchronously. a. Thrust is 5 μN. b. Thrust is 50 μN.

30 μA − 40 μA in ion beam current for A2 and B2, leading to differences in thrust values.

This test was also conducted in an open-loop control mode. Under the same thrust command, the four thrusters cannot achieve perfect identical thrust. However, the RMP is designed with thrust closed-loop control mode, wherein each thruster will output an accurate thrust value. The purpose of this test is to test the actual thrust value under open-loop control mode.

The thrust range required for "Taiji program in space" is from 5 μN to 50 μN, and the actual thrust range of RMP in "Taiji-1" is from 5 μN to 52 μN, which has meet the thrust range requirement of mission.

C. Thrust noise

The thrust noise generated by the propulsion, serving as the actuator for satellite drag-free control, has a significant impact on the measurement noise of the results. Therefore, the thrust noise requirement for the propulsion is less than 0.1 $\mu N/\sqrt{Hz}$ (10 mHz–1 Hz). The RMP in the "Taiji-1" satellite primarily undergoes thrust noise testing within the frequency range of 10 mHz to 1 Hz, due to the test time was just ten minutes, as shown in Fig. 11. In the measurement of the measurement thrust noise of the B2 thruster using GRS, the accelerometer mode was employed. The thrust was measured using the product of the measured test mass acceleration and the spacecraft mass (183 kg), rather than operating in the inertial sensing mode, meaning that there is no displacement mode involved. The measurement thrust noise of GRS was up to 2 $\mu N/\sqrt{Hz}$ (10 mHz to 1 Hz), which was far beyond the thrust noise. So in thrust noise test in-orbit, the telemetry data of screen grid voltages and beam current of the RMP are combined with computational thrust to evaluate thrust noise by Eq. (2). Therefore, the thrust noise discussed in this paper for the four RMP thrusters is the calculated thrust noise, rather than the GRS measured thrust noise. The measurement of RMP thrust noise has been completed in ground tests and is detailed in Ref. [3]. The experiment adopts the full thrusters open-loop control mode, configuring two thrust conditions where each thruster simultaneously outputs 5 μN and 50 μN.

In Fig. 11, it is observed that within the target frequency range, when the thrust is at 5 μN, the thrust noise of the A1

and A2 thrusters is less than 0.2 μN/$\sqrt{}$Hz, while the thrust noise of the B1 and B2 thrusters reaches 0.1 μN/$\sqrt{}$Hz. However, when the thrust reaches the maximum specified value of 50 μN, the thrust noise of four thrusters increases to 0.4 μN/$\sqrt{}$Hz, which is 2 to 4 times higher than that at 5 μN thrust, indicating a gradual increase in thrust noise with increasing thrust. The GRS measured thrust noise power spectral density for the B2 thruster is shown by the red line in Fig. 11(b). The measured noise in the range of 10 mHz to 1 Hz is close to 1 μN/$\sqrt{}$Hz, which is much higher than the calculated thrust noise. Therefore, thrust noise cannot be measured accurately through GRS.

This test utilizes the calculated thrust of the RMP, where thrust noise mainly originates from intrinsic factors of the RMP itself. Factors affecting the stability of thrust include radio-frequency power, propellant flow, screen grid voltage, and the emission electron of CNTN. The radio-frequency power consists of plasma absorption power and loss power inside the discharge chamber. As the temperature gradually rises after ignition, leading to changes in plasma impedance, the plasma characteristics fluctuate until the temperature stabilizes within the threshold range. The RMP employs a fixed impedance matching network, where changes in load impedance affect the power output of the radio-frequency circuit module inside the PPU, consequently influencing thrust noise. The μMFC controls the propellant flow by regulating the pressure difference across the limiting orifice. Despite designing a gas capacitor to dampen pressure fluctuations at the front end of the restricted orifice, minor fluctuations still affect thrust noise. Similarly, fluctuations in screen grid voltage impact thrust noise due to the calculated thrust is depend on the beam current and screen grid voltage in Eq. (2). In the process of ion beam and electron beam neutralization, the instability of the plume region will cause the plasma discharge fluctuation in the discharge chamber of thrusters, thereby affecting the stability of thrust. This effect tends to intensify with increasing thrust.

D. Thrust response time

Due to the limited data acquisition frequency of the RMP (12 Hz), the actual thrust response time in-orbit cannot be obtained. In this test, the thrust response time was assessed using the GRS, with a frequency of 100 Hz. However, due to the significant influence of the satellite environment on the GRS, the thrust measurement exhibited large fluctuations. Therefore, this test only analyzed the time information before and after the thrust changes. As for the actual thrust response time of the thruster in-orbit,

$$t_{TRT} = t_C + t_V, \tag{4}$$

where t_C is the time of thrust command issued to the high voltage module, and t_V is the time of screen grid voltage rising or dropping.

The B1 and B2 thrusters serve as the testing target. The double thrusters thrust output mode is employed to test the thrust response time of two thrust steps. The total thrust rises from 10 μN to 60 μN and then descends to 10 μN, as well as from 10 μN to 90 μN and then back to 10 μN, with multiple tests conducted for each thrust value. The thrust response times of thrust step were measured by GRS (in blue) and calculating (in red). But the acquisition frequency of RMP was not enough to evaluate the thrust response time. Based on the evaluation from ground-based experiments, the time from issuing the thrust command to the response of the high-voltage module was on the millisecond scale. In Fig. 12, it can be observed that the t_V is about 20 ms. Therefore, the thrust response time in this in-orbit test will be based on the results of t_V. The test revealed that both the thrust rise time and the thrust descent time are approximately 20 ms, and the magnitude of the thrust does

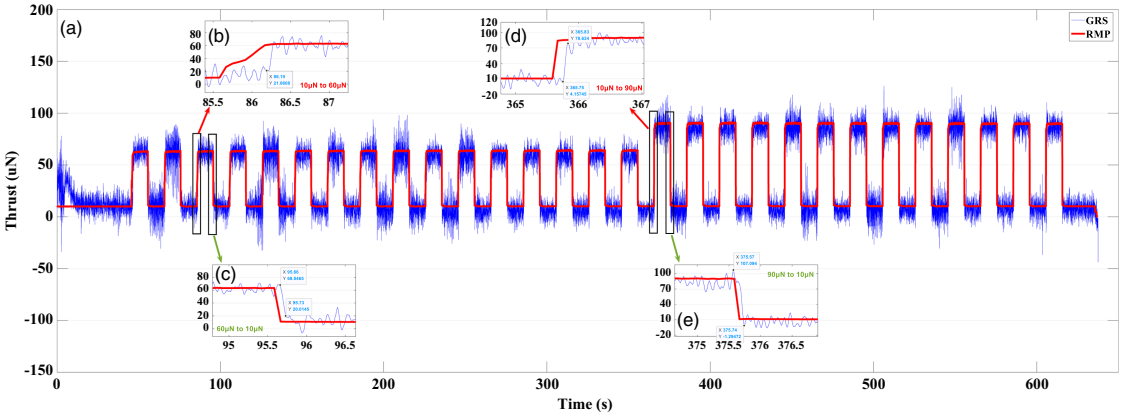

FIG. 12. Thrust response time. The red lines indicate the thrust of RMP by telemetering (12 Hz), the blue lines indicate the thrust of RMP by GRS with 100 Hz. a. Thrust square wave from 10 μN to 60 μN and from 10 μN to 90 μN. b. From 10 μN to 60 μN, thrust response time is less than 20 ms by GRS. c., From 60 μN to 10 μN, thrust response time is less than 30 ms by GRS. d. From 10 μN to 90 μN, thrust response time is less than 30 ms by GRS. e. From 90 μN to 10 μN, thrust response time is less than 30 ms by GRS.

not affect the response time. This indicates that when controlling the thrust using screen grid voltage adjustment, the voltage adjustment time is the main factor affecting thrust response time, which is the same as test on the ground.

IV. CONCLUSION

RMP as the primary propulsion of the "Taiji-1" satellite underwent thorough in-orbit performance verification. By employing pulsed propellant pressure discharge, the thrusters ignition without neutralizers before thrusters working. The success rate of thruster ignition reached 100% when meeting the ignition voltage threshold and pressure threshold. Based on in-orbit test results, the thrust range of the RMP is from 5 μN to 52 μN. At a thrust of 50 μN, the thrust noise is approximately 0.4 $\mu N/\sqrt{Hz}$ (10 mHz–1 Hz), which is 2 to 4 times higher compared to low-thrust output levels (5 μN). The thrust response time reached 20 ms. The characterization of RMP in orbit has reached the expectations of Taiji-1 satellite mission. Although the in-orbit performance of the RMP (thrust noise, thrust resolution, and lifetime) currently falls short of meeting the final requirements of the "Taiji Program in space," the gaps are within 1order of magnitude. The performance is inevitably influenced by propulsion itself, emphasizing the necessity of further enhancing the stability and efficiency of the PPU and μMFC. Additionally, the life performance requires further validation.

ACKNOWLEDGMENTS

The authors would like to acknowledgement the Taiji Program Team, the Engineering Team, and the Satellite Platform Team for the chance of verifying in-orbit of RMP. This research was supported by the National Key R&D Program of China (Grant No. 2021YFC2202800), Strategic Priority Research Program of the Chinese Academy of Sciences (Grant No. XDA1502070901), and Youth Innovation Promotion Association CAS (Grant No. 2023022).

[1] W. R. Hu and Y. L. Wu, The Taiji program in space for gravitational wave physics, and the nature of gravity, Natl. Sci. Rev. **4**, 685 (2017).
[2] Z. R. Luo, M. Zhang, G. Jin *et al.*, Introduction of Chinese space-borne gravitational wave detection program "Taiji" and "Taiji-1" satellite mission, J. Deep Space Explor. **7**, 3 (2020).
[3] J. W. He, L. Duan, and Q. Kang, Ground performance tests and evaluation of RF ion microthrusters for Taiji-1 satellite, Int. J. Mod. Phys. A **36**, 2140014 (2021).
[4] H. Liu, X. Niu, M. Zeng, S. Wang, K. Cui, and Daren Yu, Review of micro propulsion technology for space gravitational waves detection, Acta Astronaut. **193**, 496 (2022).
[5] M. Armano, H. Audley, J. Baird *et al.*, LISA pathfinder micronewton cold gas thrusters: In-flight characterization, Phys. Rev. D **99**, 122003 (2019).
[6] J. K. Ziemer, C. Marrese-Reading, S. M. Arestie *et al.*, LISA colloid microthruster technology development plan and progress, *Vienna: 36th International Electric Propulsion Conference* (2019).
[7] G. Anderson, J. Anderson, M. Anderson *et al.*, Experimental result from the ST7 mission on LISA Pathfinder, Phys. Rev. D **98**, 102005 (2018).
[8] S. Y. Xu, L. X. Xu, L. X. Cong, Y.-G. Li, and C.-F. Qiao, First result of orbit verification of Taiji-1 Hall micro thruster, Int. J. Mod. Phys. A **36**, 2140013 (2021).
[9] J. Luo, Y. Z. Bai, L. Cai *et al.*, The first round result from the TianQin-1 satellite, Classical Quantum Gravity **37**, 185013 (2020).
[10] H. W. Loeb, S. W. Weis, D. Feili *et al.*, Development of RIT-microthrusters, *Vancouver: 55th International Astronautical Congress* (2004).
[11] H. W. Loeb, Recent work on radio frequency ion thrusters, J. Spacecr. Rockets **8**, 494 (1971).
[12] R. Dmytro, M. Javier, H. Lui *et al.*, In-orbit demonstration of an iodine electric propulsion system, Nature (London) 599, 411 (2021).
[13] D. D. Cara, S. Strandmoe, J. A. Romera Perez *et al.*, RIT micrpropulsion system on LISA pathfinder, *Wiesbaden: 32nd International Electric Propulsion Conference* (2011).
[14] 1 cm RF Ion Thruster BIT-1, Busek, 2015.
[15] Z. Q. Hu, P. C. Wang, J. F. Deng *et al.*, The drag-free control design and in-orbit experimental results of "Taiji-1", Int. J. Mod. Phys. A **36**, 2140019 (2021).
[16] J. W. He, P. Liu, R. L. Gao, C. Xue, L. Ma, L. Duan, and Q. Kang, Research on the neutralization control of the RF ion micropropulsion system for the "Taiji-1" satellite mission, Plasma Sci. Technol. **22**, 094002 (2020).
[17] A. Kuchler, *Voltage Engineering Fundamentals ·Technology·Applications* (Springer, New York, 2017).
[18] L. F. Ma, L. Duan, J. W. He, and Q. Kang, The impact of neutralizer-free ignition of a radio frequency ion thruster on the lifetime of the ion optics system, Int. J. Mod. Phys. A **36**, 2140017 (2021).
[19] H. D. Li and Z. Wang, Implementation of high-precision inertial reference for Taiji-1 satellite and its ground evaluation based on torsion pendulum system, Int. J. Mod. Phys. A **36**, 2140010 (2021).